

Exploring Cell-to-Cell Interactions (CCI) Within GABAergic Interneurons During Development

Ali Balubaid, Ana Cecilia, Azari Bantan, Daniel Soto

Date: 06-05-2024

**BESE394 Final Project
(Report)**

Introduction:

The advent of single-cell technologies and the availability of comprehensive ligand-receptor (L-R) interaction databases have facilitated the analysis of cell-to-cell interactions (CCI). Most analytical frameworks assess the likelihood of specific interactions occurring based on the expression levels of ligands and receptors within both source and target cell clusters, enabling a detailed examination of cell-to-cell interactions¹. However, comparing different tools poses challenges due to the varied statistical strategies used by them². Such strategies include permutation of cluster labels, regularization techniques, and scaling methods, some of which prioritize interactions based on input datasets they were designed for. These diverse approaches can yield disparate outcomes and contrasting results across analyses. To provide a rather standard workflow when it comes to analyzing the cell interactome, LIANA was proposed as a method to decouple the method from its paired database source, generating a unified output across different methods³. To do so, LIANA re-implements such methods to generate an internal scoring function for each interaction generated by every method-source combination. LIANA gets the CCI information using OmnipathR and then formats the data appropriately to be used by the method analyzed. Lastly, it generates consensus ranks that are aggregated to visualize the results from all the methods used in the analysis.

Since CCI analysis is based on single-cell RNA-seq (scRNA-seq) technology, it becomes very useful to analyze heterogeneous cellular populations like those found in the brain. Specifically, the cortical tissue of the brain harbors two populations of cells: neural and non-neural cells. Neural cells, those in charge of information transmission through synapses, can be further classified as either excitatory or inhibitory, depending on the kind of released neurotransmitters. Inhibitory cells include GABAergic cells, which depending on the expression of a molecular mark and its targeting compartment inside the brain, can be further classified as cells expressing: parvalbumin (*Pvalb*), somatostatin (*Sst*), vasoactive intestinal peptide (*Vip*) and lysosome-associated membrane protein (*Lamp5*)⁴. Such diversity of interconnected and heterogeneous populations of cells allows the human brain to perform complex tasks.

Here, we use LIANA³ to predict the L-R interactions between different cell populations of the mouse developing brain cortex. Our analysis focuses on two key developmental time-points: postnatal days 10 (p10) and 28 (p28).

Methods:

In this project, we analyzed samples derived from a previous work by Allaway et. al⁵, in which brain cortical interneuron cell nuclei were isolated from mice in development stages P10 and P28.

For our analysis, we implemented a pipeline that could be categorized into three main steps (1) assembling and preprocessing scRNAseq data, (2) inferring CCI through a bootstrapped LIANA framework, (3) Functional characterization and visualization results for downstream interpretation. We present our pipeline in Figure 1.

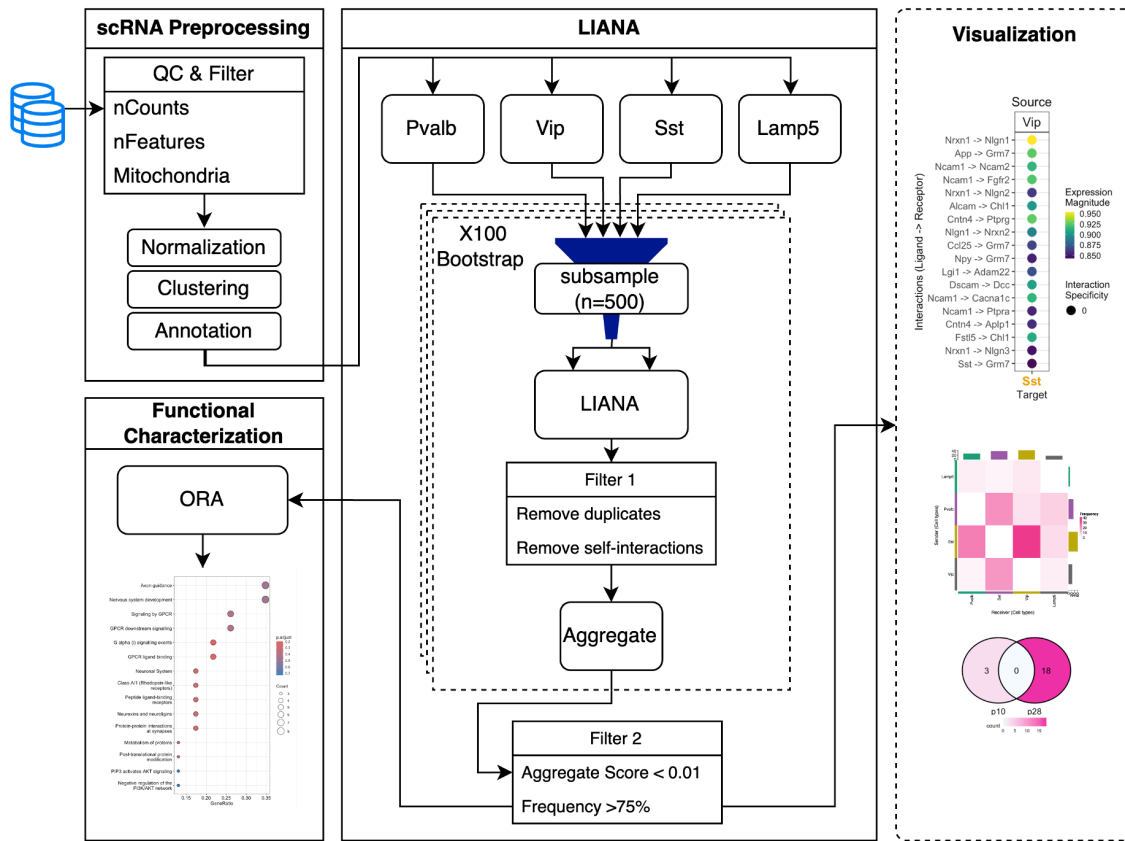


Figure 1: Schematic representation shows steps taken in the pipeline. QC: Quality Control; ORA: over-representation analysis.

scRNaseq Preprocessing

Processed raw scRNA-seq data using the standard CellRanger v3.0.0 pipeline (10x Genomics) was loaded from GEO. Further processing of the raw count data was applied using the Seurat R package (v5)⁶. Dataset from each developmental stage (p10 and p28) were merged to facilitate downstream analysis. Cells were filtered based on the distributions of mitochondrial ratio (<10%), number of features (1k–8k genes), and number of counts (2k–7k reads). Post filtering, the data was normalized (`NormalizeData()`), top 2k variable features were identified (`FindVariableFeatures()`), then scaled (`scale.data()`), and dimensionally reduced (`RunPCA()`). The K-nearest neighbor graph was constructed using the top 30 PCA dimensions, followed by graph-based clustering using the “Louvain” algorithm (`FindNeighbors()` and `FindClusters()`, respectively). Cells were annotated with Azimuth using the

‘mousecortexref’ as a reference⁷. Clustered and annotated cells were visualized on UMAP. For more details, please

LIANA Pipeline

The preprocessed scRNAseq data was sub-grouped into 4 cell populations of interest: *Pvalb*, *Sst*, *Vip* and *Lamp5*. The LIANA (v.0.1.13) package and MouseConsensus resource were utilized to infer CCIs from the gene expression of each cell population, using three re-implemented liana methods (CellChat⁸, CellphoneDB⁹, and SingleCellSignalR¹⁰), along with providing a consensus via `liana_aggregate()` function. The selection of the three methods was based on recommendations from a separate study that utilized a comparable dataset from the mouse visual cortex². Random sampling (n=500) of cells from each population were selected to run LIANA. Here, we focused on direct interactions between different cell populations, excluding self-interactions. Duplicated interactions were also removed. To retain robust interactions, two-fold filtrations were implemented: filtering results by 1) `aggregate_rank` score (`aggregate_rank < 0.01`), and 2) selecting interactions that occurred >75% across the bootstrapped results (N=100). Overall, the aforementioned steps were applied on the 4 cell populations at both developmental stages, P10 and P28 separately, retaining robust interactions which were used for subsequent analysis (i.e., ORA; see below).

Functional Characterization

The functional characterization was carried out, taking into account the stage of development and direction of the interaction. Firstly, we randomly selected one output of LIANA out of the 100 outputs obtained from the bootstrap step, which contained the robust interactions identified at developmental stages: P10 and P28. Then, we subsetted LIANA outputs to isolate unique and shared interactions at each developmental stage (the number of interactions per category is visualized using `ggVennDiagram()`). To visualize these interactions by source and target cells, depicting their L-R pairs and specificities, we generated dot plots using the `Liana_dotplot()` function from the LIANA package (v.0.1.13). Furthermore, the ReactomePA package (v.1.46.0) was utilized to perform an over-representation analysis (ORA) to identify enriched pathways associated with the identified L-R interactions. We define our L-R

geneset for each pair of interacting cell subclasses while accounting for their directionality and categorizing them based on whether they are shared or unique to either p10 or p28. We employed all possible ligands and receptors expressed by all interacting cell subclass pairs as the background.

Code and Data Availability

Raw scRNA-seq count data can be found in GEO using the following IDs: GSM5014306 and GSM5014308, for the two time-points, p10 and p28, respectively. More details on the QC and analysis could be found on the markdown supplemented in the Github repository. Additionally, the scripts for scRNA-seq processing, LIANA, and functional characterization analysis are available at:

https://github.com/anagonzalezalvarez/Bioinformatics_Pipelines/tree/main/Project

Results & Discussion

We performed a CCI analysis for interneuronal cells sampled from the developing brain cortex of mice in development stages P10 and P28. Specifically, we evaluated the interactions between inhibitory GABAergic cells identified as *Pvalb*, *Sst*, *Vip*, and *Lamp5*. From this analysis, we determined two sources of frequent interactions: between *Sst* and *Vip* cells and between *Sst* and *Pvalb* cells (Figure 2). The fact that *Sst* and *Pvalb* share a higher frequency of interactions compared to other cellular populations during P10 is supported by previous reports that indicate that in developing mice, those are the most prevalent populations of cells in the brain cortex, even sharing a common embryonic origin¹¹.

Interestingly, a higher interaction frequency was observed at a later stage of development (p28) between *Sst* and *Vip* cells across both directions, with few or no persistent interactions from early development (Figure 3A). On the other hand, most interactions between *Sst* and *Pvalb* persist from early to late development, with slightly higher interactions observed at an early stage (Figure 3B). The results obtained are reinforced by the fact that *Vip* cells have been reported to be present in higher numbers in later stages of development. Furthermore, they have a crucial

role in the GABAergic interneuronal circuitry due to their ability to inhibit *Sst* cells, playing a more disinhibitory role¹². Lastly, dysregulation of *Vip* cells has been shown to impair the development of cortical cells by inducing changes in their activity and temporal organization¹³.

Regarding the interactions between *Sst* and *Vip*, we observe high *Nrxn1* targeting *Nlgn1* interactions in stage P10 for *Sst* targeting *Vip*. This is reversed during stage P28, with *Nlgn1* targeting *Nrxn1* in stage P28 (Figure 4A). While predominant in stage 10, neurexins and neuroligins signaling is diminished in P28. It is mainly substituted with GPCR pathway-associated L-R pairs in stage P28. MAPK pathway is enriched in both P10 and P28 (Figure 4B). Since *Nrxn1-Nlgn1* interaction is bidirectional, it is not surprising that their inverse is observed for *Vip* ligands targeting *Sst* receptors (Figure 5A). We also observe high neurexin and neuroligin expression in stage P10 and increased enrichment of GPCR pathway-associated L-Rs in stage P28 (Figure 5B). This suggests that L-R pairs between *Sst* and *Vip* are more stage-specific rather than neuronal subclass-specific. This is further supported by the reduced or absent shared L-R pairs.

Another subclass pair with notable changes in their interaction frequency are *Sst* and *Pvalb*. The analysis of CCI reveals the predominant presence L-R pairs associated with cellular proliferation and cell migration. This becomes evident due to the presence of the receptor FGFR2 in both *Sst* to *Pvalb* interactions (Figure 6A) and *Pvalb* to *Sst* interactions (Figure 7A) in a stage-independent manner. A similar observation can be made for the ligand SLIT2, which has a relevant role in the migration and formation of neuronal circuits and was found to interact with multiple receptors to achieve such cellular coordination¹⁴.

The *Sst* signaling directed at *Pvalb* mainly relates to protein synthesis and metabolism (Figure 6B). We also see an enrichment for L-R associated with extracellular matrix organization in P10, whereas P28 has more MAPK signaling pathway-related L-Rs (Figure 6B). As for *Pvalb* signaling to *Sst* neurons, it relies on ROBO, MAPK, GPCR, and Tyrosine Kinase signaling (Figure 7B). Between the stages, we see decreased reliance on the ROBO and MAPK signaling pathways and more L-R associated with Tyrosine Kinase and MAPK signaling pathways (Figure 7B). Our results show a dynamic change in the stage-specific functionality of *Sst* to *Pvalb*

interactions but a preservation of *Pvalb* to *Sst* signaling across stages. Previous studies have shown that *Sst* maturation precedes *Pvalb*, which could explain the dynamic changes across stages for *Pvalb* ligand release¹¹. Furthermore, disruption of *Sst* cells in early-born individuals have shown to impair the synaptic maturation of infragranular *Pvalb* interneurons¹⁵.

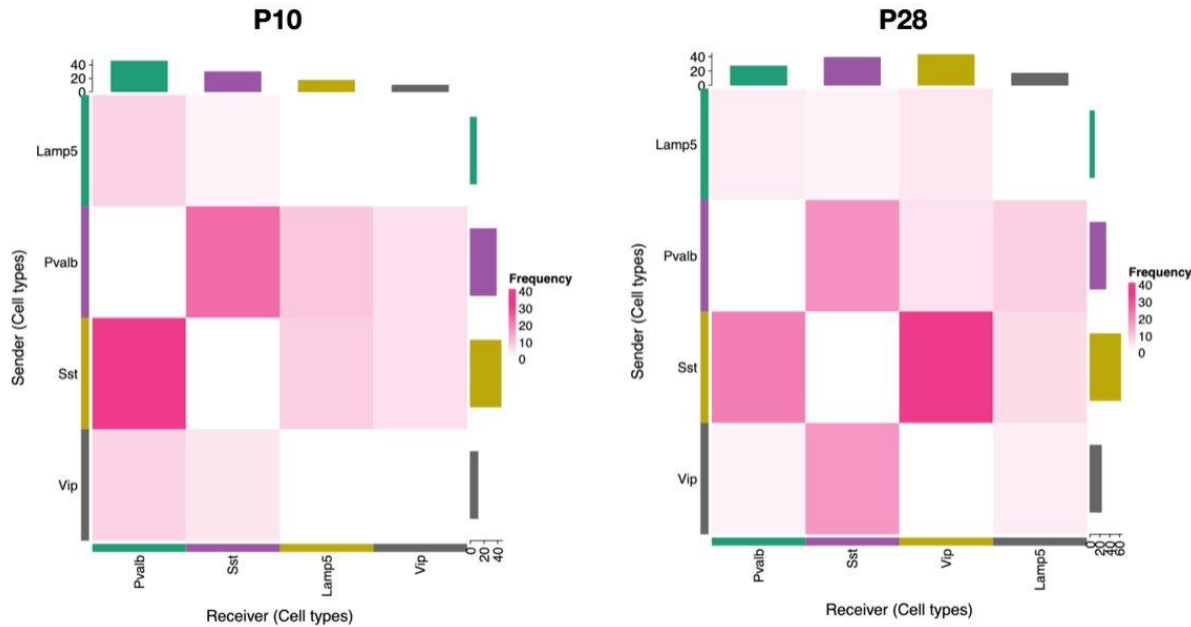


Figure 2. Interaction Frequency heatmap between GABAergic Neurons: The heatmap shows the interaction frequency between the GABAergic cell type subclasses annotated by their marginal abundance. The panels show the interactions during period P10 (left) and P28 (right).

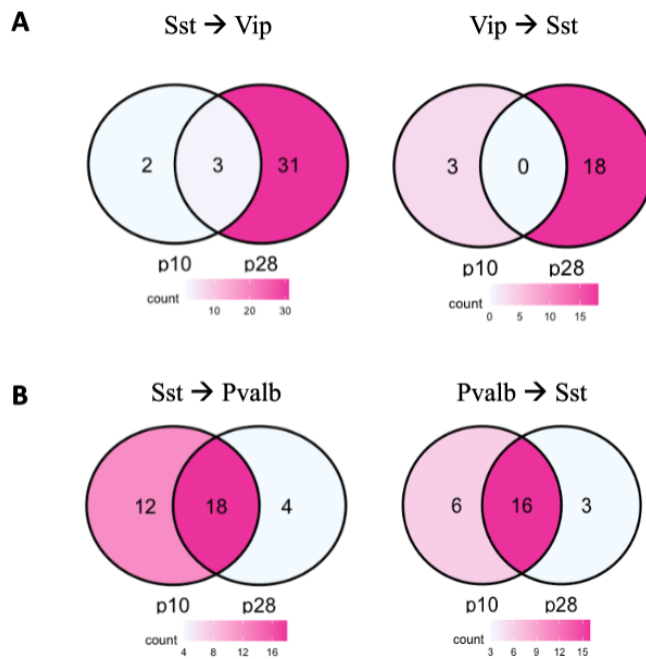


Figure 3. Unique and shared (intersect) interactions at early (p10) and late (p28) stages of development across interacting cell populations of interest: A) $\text{Sst} \longleftrightarrow \text{Vip}$, and B) $\text{Sst} \longleftrightarrow \text{Pvalb}$.

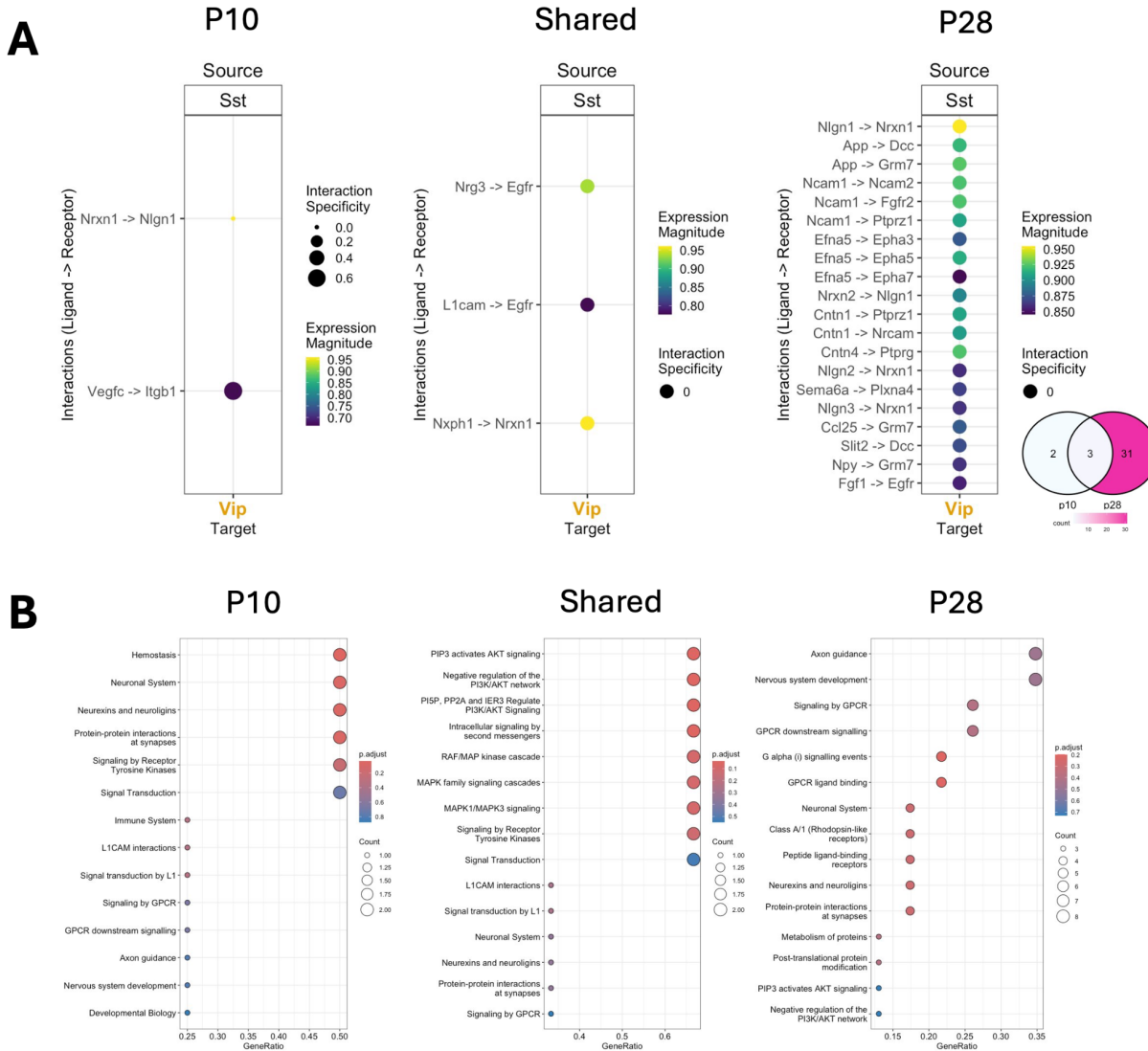


Figure 4. Cell-to-Cell Interactions and Functional Enrichment from Sst to Vip: A. Sst Ligand to Vip receptor pairs for only P10 (left), only P28 (right), and their intersect (middle), as highlighted in the venn diagram at the bottom right. Each panel shows the specificity and the magnitude of the interaction. B. Functional enrichment of the ligand-receptor pairs for only P10 (left), only P28 (right), and their intersect (middle). Each panel shows the significance and the number of abundance of the GO term.

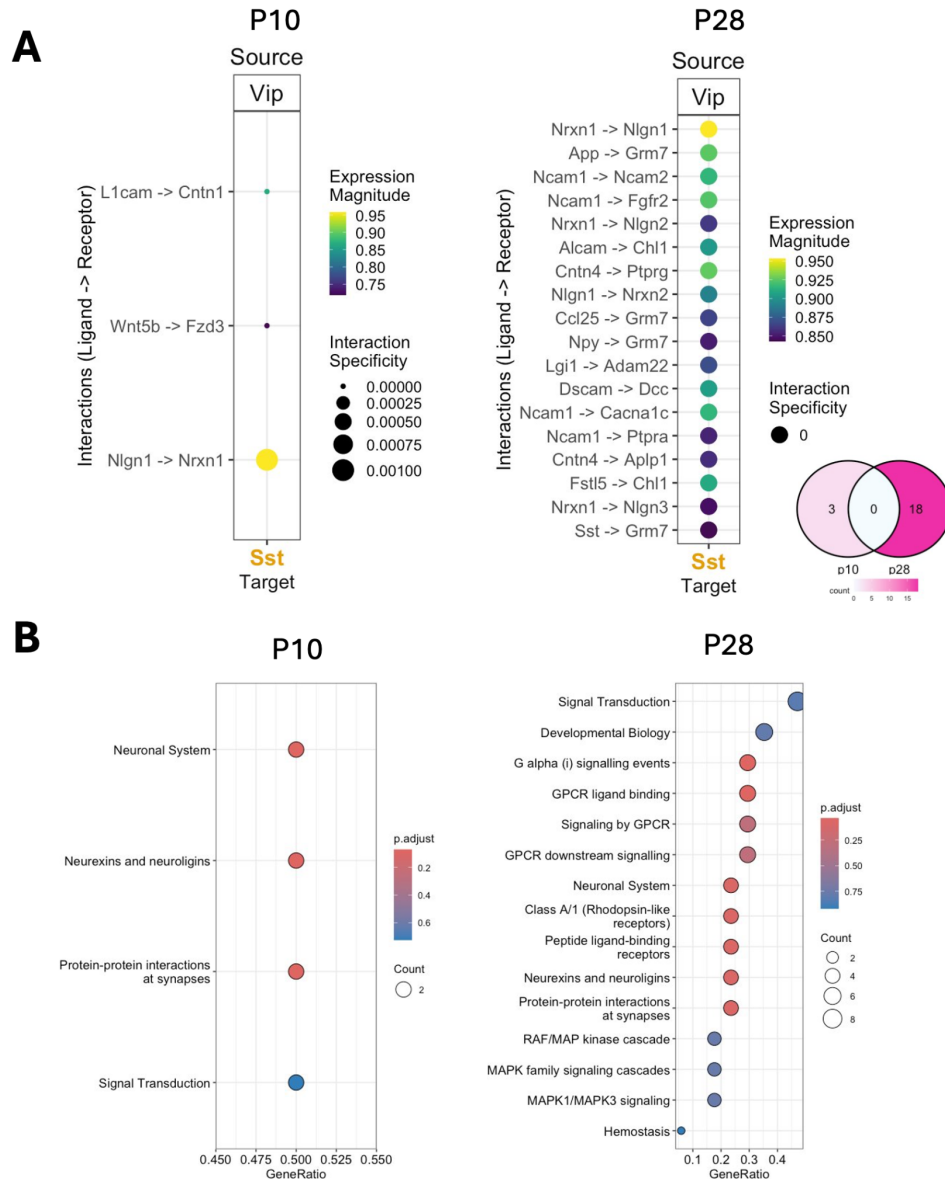


Figure 5. Cell-to-Cell Interactions and Functional Enrichment from *Vip* to *Sst*: A. *Vip* Ligand to *Sst* pairs for P10 (left) and P28 (right), as highlighted in the venn diagram at the bottom right. Each panel shows the specificity and the magnitude of the interaction. B. Functional enrichment of the ligand-receptor pairs for P10 (left) and P28 (right). Each panel shows the significance and the number of abundance of the GO term.

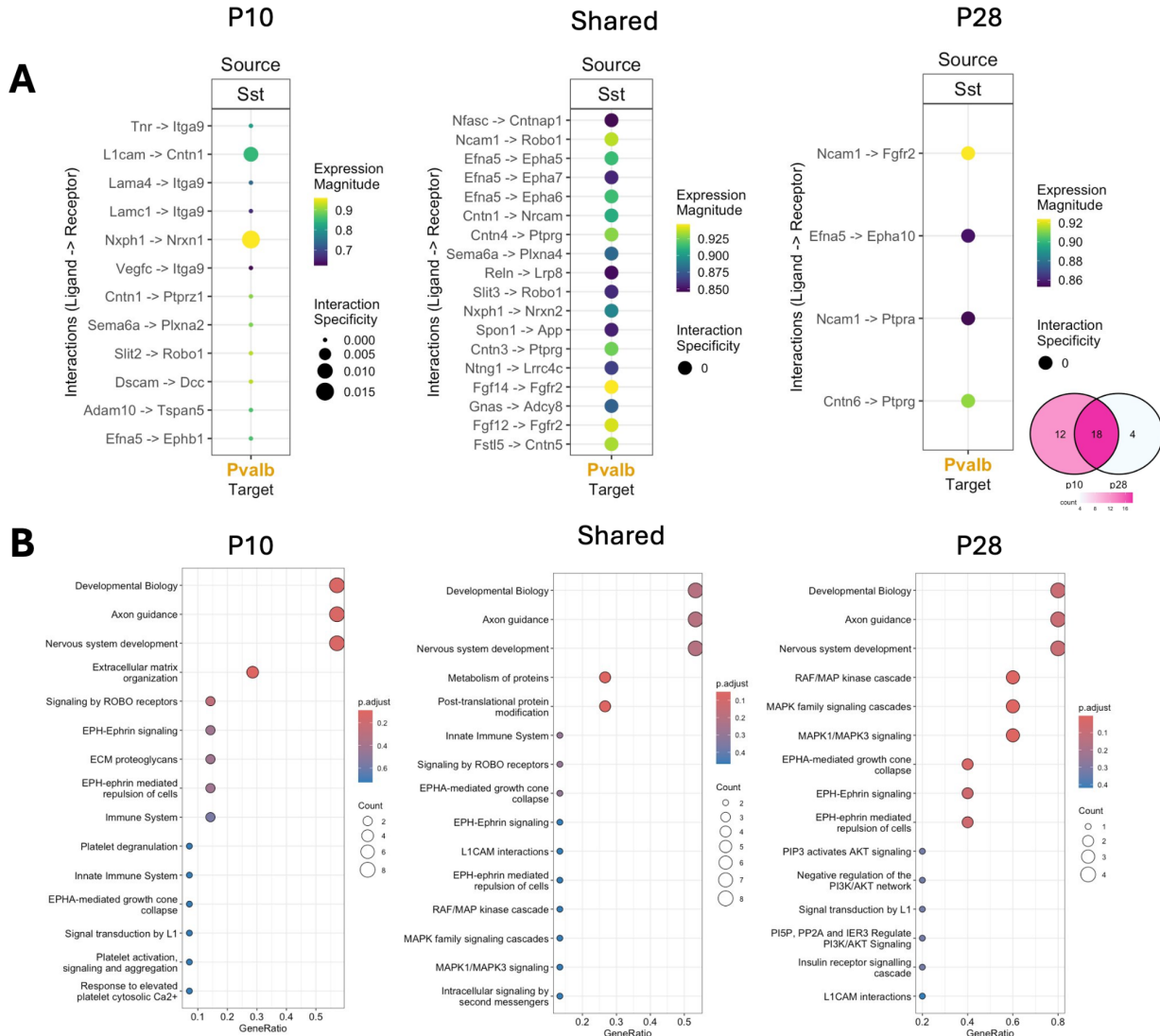


Figure 6. Cell-to-Cell Interactions and Functional Enrichment from Sst to Pvalb: A. Sst Ligand to Pvalb pairs for only P10 (left), only P28 (right), and their intersect (middle), as highlighted in the venn diagram at the bottom right. Each panel shows the specificity and the magnitude of the interaction. B. Functional enrichment of the ligand-receptor pairs for only P10 (left), only P28 (right), and their intersect (middle). Each panel shows the significance and the number of abundance of the GO term.

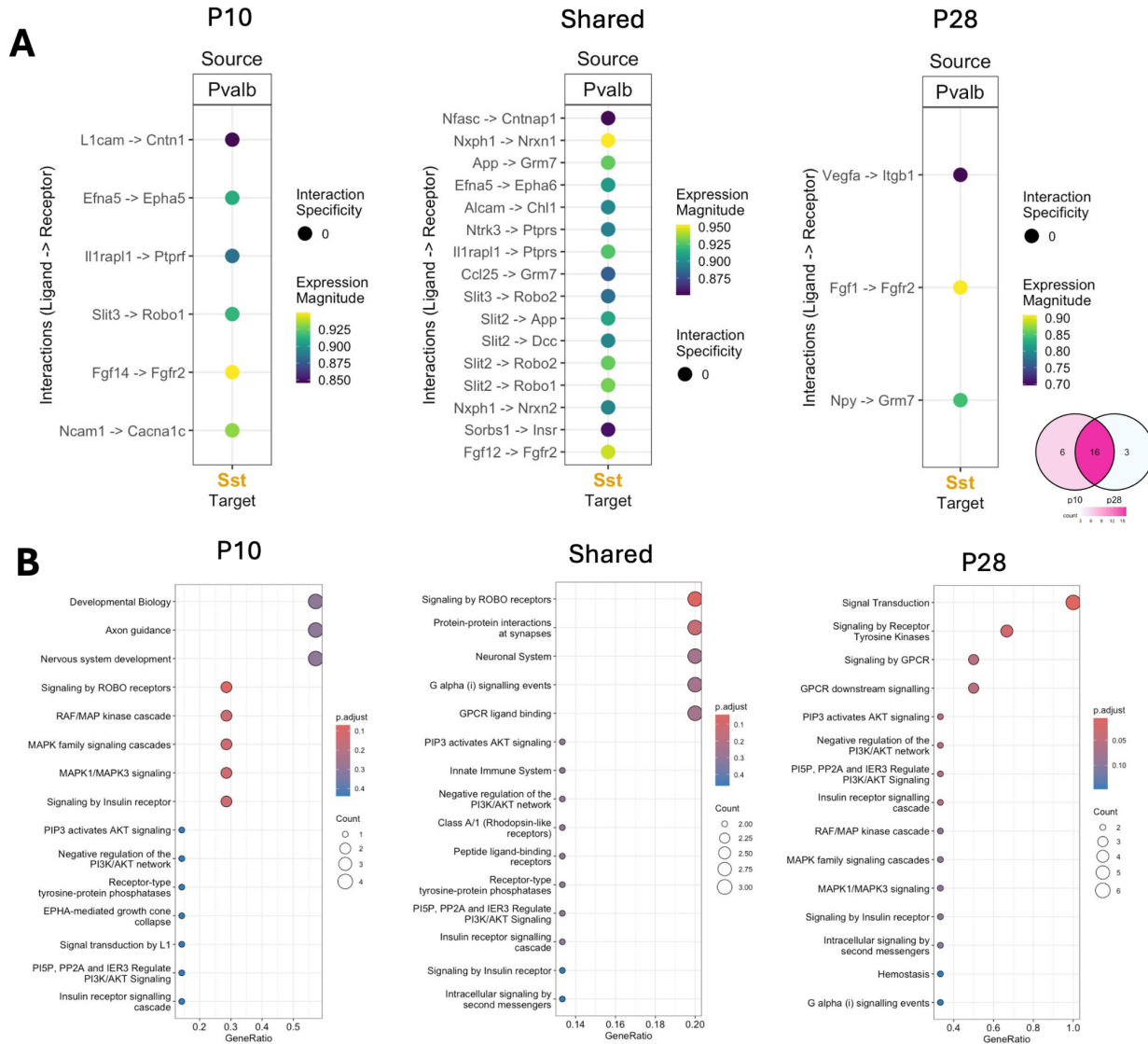


Figure 7. Cell-to-Cell Interactions and Functional Enrichment from *Pvalb* to *Sst*: A. *Pvalb* Ligand to *Sst* pairs for only P10 (left), only P28 (right), and their intersect (middle), as highlighted in the venn diagram at the bottom right. Each panel shows the specificity and the magnitude of the interaction. B. Functional enrichment of the ligand-receptor pairs for only P10 (left), only P28 (right), and their intersect (middle). Each panel shows the significance and the number of abundance of the GO term.

Conclusion

In the developing mouse brain cortex, our single-cell CCI analysis of inhibitory GABAergic cells at stages P10 and P28 revealed increased interaction frequency between *Sst* and *Vip* cells at P28, while interactions involving *Sst* and *Pvalb* cells persisted predominantly from early to late development. As expected, most of the *Sst* and *Vip* interactions are associated with developmental processes such as synaptic differentiation and extracellular organization. *Sst* and *Pvalb* interactions on the other hand relate more to different signaling pathways, with stage specific changes differing in the pathways of signaling. These observations provide a clear connection between the functional role of persistent versus transient neuronal subclass interactions.

Previous studies report that neurexins trigger postsynaptic differentiation, whereas neuroligins trigger presynaptic differentiation¹⁶. Given our observations of the neurexin-neuroligin stage-specific dynamics between *Sst* and *Vip*, *Vip* cells are likely post-synaptic in relation to *Sst* in earlier stages. In later stages (P28), however, there is a shift, with more pre-synaptic *Vip* subclasses. This could guide further studies into the organizational dynamics of *Sst* and *Vip* during the development of the primary visual cortex.

However, when considering the limitations and future directions of our study, it's important to note that we only examined two specific stages of brain development (p10 and p28), limiting our insights into the dynamic changes occurring throughout cortical development. Moreover, while the experimental design of the dataset analyzed in this study was enriched for inhibitory neuron subtypes, future investigations could benefit from expanding this focus to encompass other subclasses, including the excitatory neurons. Additionally, integrating spatial data, possibly by the implementation of LIANA+, we could further investigate the distance between interacting cells, providing a more detailed understanding of both short and long-range interactions.

Bibliography

1. Armingol, E., Officer, A., Harismendy, O. & Lewis, N. E. Deciphering cell–cell interactions and communication from gene expression. *Nat. Rev. Genet.* **22**, 71–88 (2021).
2. Liu, Z., Sun, D. & Wang, C. Evaluation of cell-cell interaction methods by integrating single-cell RNA sequencing data with spatial information. *Genome Biol.* **23**, 218 (2022).
3. Dimitrov, D. *et al.* Comparison of methods and resources for cell-cell communication inference from single-cell RNA-Seq data. *Nat. Commun.* **13**, 3224 (2022).
4. Wu, S. J. *et al.* Cortical somatostatin interneuron subtypes form cell-type-specific circuits. *Neuron* **111**, 2675-2692.e9 (2023).
5. Allaway, K. C. *et al.* Genetic and epigenetic coordination of cortical interneuron development. *Nature* **597**, 693–697 (2021).
6. Hao, Y. *et al.* Dictionary learning for integrative, multimodal and scalable single-cell analysis. *Nat. Biotechnol.* **42**, 293–304 (2024).
7. Hao, Y. *et al.* Integrated analysis of multimodal single-cell data. *Cell* **184**, 3573-3587.e29 (2021).
8. Jin, S. *et al.* Inference and analysis of cell-cell communication using CellChat. *Nat. Commun.* **12**, 1088 (2021).
9. Efremova, M., Vento-Tormo, M., Teichmann, S. A. & Vento-Tormo, R. CellPhoneDB: inferring cell–cell communication from combined expression of multi-subunit ligand–receptor complexes. *Nat. Protoc.* **15**, 1484–1506 (2020).
10. Cabello-Aguilar, S. *et al.* SingleCellSignalR: inference of intercellular networks from single-cell transcriptomics. *Nucleic Acids Res.* **48**, e55 (2020).
11. Tuncdemir, S. N. *et al.* Early Somatostatin Interneuron Connectivity Mediates the Maturation of Deep Layer Cortical Circuits. *Neuron* **89**, 521–535 (2016).
12. Ferrer, C. & De Marco García, N. V. The Role of Inhibitory Interneurons in Circuit Assembly and Refinement Across Sensory Cortices. *Front. Neural Circuits* **16**, (2022).
13. Batista-Brito, R. *et al.* Developmental Dysfunction of VIP Interneurons Impairs Cortical Circuits. *Neuron* **95**, 884-895.e9 (2017).
14. Bielle, F. *et al.* Slit2 Activity in the Migration of Guidepost Neurons Shapes Thalamic Projections during Development and Evolution. *Neuron* **69**, 1085–1098 (2011).

15. Wang, C.-Z. *et al.* Early-generated interneurons regulate neuronal circuit formation during early postnatal development. *eLife* **8**, e44649 (2019).
16. Craig, A. M. & Kang, Y. Neurexin–neuroligin signaling in synapse development. *Curr. Opin. Neurobiol.* **17**, 43 (2007).